Late Pleistocene tropical Pacific temperature sensitivity to radiative greenhouse gas forcing

Kelsey A. Dyez[1] and A. Christina Ravelo[2]
[1]Department of Earth and Planetary Sciences, University of California–Santa Cruz, Santa Cruz, California 95064, USA
[2]Department of Ocean Sciences, University of California–Santa Cruz, Santa Cruz, California 95064, USA

ABSTRACT

Understanding how global temperature changes with increasing atmospheric greenhouse gas concentrations, or climate sensitivity, is of central importance to climate change research. Climate models provide sensitivity estimates that may not fully incorporate slow, long-term feedbacks such as those involving ice sheets and vegetation. Geological studies, on the other hand, can provide estimates that integrate long- and short-term climate feedbacks to radiative forcing. Because high latitudes are thought to be most sensitive to greenhouse gas forcing owing to, for example, ice-albedo feedbacks, we focus on the tropical Pacific Ocean to derive a minimum value for long-term climate sensitivity. Using Mg/Ca paleothermometry from the planktonic foraminifera *Globigerinoides ruber* from the past 500 k.y. at Ocean Drilling Program (ODP) Site 871 in the western Pacific warm pool, we estimate the tropical Pacific climate sensitivity parameter (λ) to be 0.94–1.06 °C (W m^{-2})$^{-1}$, higher than that predicted by model simulations of the Last Glacial Maximum or by models of doubled greenhouse gas concentration forcing. This result suggests that models may not yet adequately represent the long-term feedbacks related to ocean circulation, vegetation and associated dust, or the cryosphere, and/or may underestimate the effects of tropical clouds or other short-term feedback processes.

INTRODUCTION

Greenhouse gas (GHG) forcing directly and indirectly affects sea-surface temperature (SST) on geologic time scales (Lea, 2004; Hansen and Sato, 2012) yet remains a key uncertainty for estimating future climate change (Knutti and Hegerl, 2008). Models estimate global equilibrium temperature changes of ~2–4.5 °C due to doubled CO_2, but do not fully account for 'slow' feedbacks (e.g., those involving deep ocean circulation, vegetation, dust, or ice sheets); thus, the range of potential long-term warming may fall outside the range indicated by models (Knutti and Hegerl, 2008). Geological paleoclimate studies provide estimates of tropical equilibrium climate system sensitivity, the SST change associated with CO_2 and CH_4 radiative forcing including all fast and slow internal climate feedbacks (Lea, 2004). Thus, our definition of climate sensitivity is the SST change associated with a given GHG forcing once other internal feedbacks (e.g., aerosol, dust, cloud) have been allowed to propagate. This empirical method implicitly accounts for all feedbacks to GHG forcing. As previously defined, this relationship between SST and GHG forcing is the past equilibrium climate sensitivity parameter (λ), in °C (W m^{-2})$^{-1}$ (Otto-Bliesner et al., 2009; Lea, 2004).

Models tend to agree on the amount of temperature change in the tropics for the Last Glacial Maximum (LGM; Otto-Bliesner et al., 2009) and future warming scenarios (DiNezio et al., 2009), making tropics data-model comparisons less model-dependent. Also, the tropics are not subject to ice-albedo feedbacks, which increase climate sensitivity at the high latitudes (e.g., Holland and Bitz, 2003). Thus, tropical climate sensitivity provides a firm 'lower bound' for global climate sensitivity without the confounding effects of high-latitude feedbacks.

Although model-derived past tropical climate sensitivity [0.67–0.83 °C (W m^{-2})$^{-1}$] generally agrees with observational estimates (e.g., Otto-Bliesner et al., 2009; Schmittner et al., 2011), some models tend to rely on the Multiproxy Approach for the Reconstruction of the Glacial Ocean Surface (MARGO) SST reconstruction (Waelbroeck et al., 2009). Particularly in the tropical Pacific, MARGO is based largely on SSTs derived from foraminiferal assemblage distributions, which are commonly biased by ecological shifts (Mix et al., 2001) and more strongly correlated with mixed-layer and thermocline depth than SST (Andreasen and Ravelo, 1997). Geochemical SST reconstructions from the tropical Pacific show a larger amplitude of glacial-interglacial change (e.g., Medina-Elizalde and Lea, 2005) and represent a more accurate indicator of past climate sensitivity than foraminifera transfer functions in the tropics (Lea, 2004).

Excellent spatial coverage of the tropical Pacific on orbital timescales is not possible with available cores; thus, our approach is to generate a high-quality geochemical SST record in an important section of the tropical oceans. The western equatorial Pacific warm pool covers a large area of the surface ocean, plays an important role in atmospheric convection, and gives an overall sense of tropical climate sensitivity. Also, the most desirable record has not been subject to the dynamic effects associated with equatorial upwelling or proximity to strong SST gradients that existing records may have experienced, and includes multiple glacial cycles to provide many realizations of warm and cold extremes in climate and in greenhouse gas concentrations. Finally, the ideal site is in relatively shallow water to minimize the high-Mg-calcite dissolution associated with deeper waters. For these reasons, we selected Ocean Drilling Program (ODP) Site 871 in the western Pacific. Its location (5°33.1'N, 172°20.7'E; Fig. 1) is far from sharp modern oceanographic gradients and its depth (1255 m) is shallower than other records and well above the lysocline (Shipboard Scientific Party, 1993), ideal for Mg/Ca-based SST estimates.

The Mg/Ca paleotemperature technique is based on the temperature dependence of Mg substitution in calcite (e.g., Anand et al., 2003), though calcite with higher Mg/Ca composition preferentially dissolves from carbonate shells at depth, decreasing the original Mg/Ca value. Most attempts to correct for this effect (e.g., Dekens et al., 2002), add a linear dissolution correction after calculating SST with the expo-

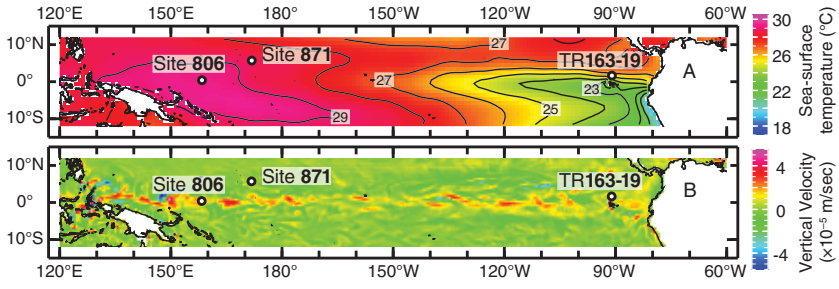

Figure 1. Location map for three core locations: Ocean Drilling Program (ODP) Site 806, ODP Site 871, and core TR163-19. Mapped are modern average sea-surface temperature (A) (Locarnini et al., 2010), and vertical velocity at 25 m water depth for the month of July 2000 (B) (Carton and Giese, 2008).

nential relationship, which overestimates the associated range of temperature variability. Correcting the Mg/Ca value for dissolution before applying the Mg/Ca-temperature relationship (after Rosenthal and Lohmann, 2002) is a more reasonable technique to constrain the amplitude of SST change in the tropical warm pool and to formulate a lower bound for climate sensitivity. We use this method to demonstrate that late-Pleistocene equatorial Pacific SST climate sensitivity is higher than most models predict.

METHODS AND APPROACH

A new dissolution-corrected *Globigerinoides ruber* Mg/Ca SST record for the past 500 k.y. from western tropical Pacific ODP Site 871 was compared to published records of GHG concentrations from air bubbles trapped in ice cores (Siegenthaler et al., 2005; Loulergue et al., 2008) to calculate past climate sensitivity. For age model control, the benthic $\delta^{18}O$ stratigraphy for Site 871 was aligned with a benthic $\delta^{18}O$ stack (Lisiecki and Raymo, 2005; see the GSA Data Repository[1]). The glacial-interglacial amplitude of both records is ~2.0‰. Sediment representing the most recent 43 k.y. of the record was disturbed in the coring process and is removed from further analysis.

To correct for high-Mg calcite dissolution at depth, we assigned a depth-dependent correction to the measured Mg/Ca value (after Rosenthal and Lohmann, 2002) before applying the exponential Mg/Ca-SST calibration. The depth-dependent correction for *G. ruber* is derived from calculating the residual between published core-top Mg/Ca data from the tropical warm pool regions and calculated surface Mg/Ca values at each core-top location. Since no dissolution is likely in surface waters, this correction should not be extended to <~600 m water depth without additional data. We derived a new *G. ruber* equation for tropical Pacific SST,

$$\mathrm{SST} = \ln[(\mathrm{Mg/Ca}_{\mathrm{measured}} + 0.259 \times \mathrm{depth(km)} + 0.537) / 0.38] / 0.09, \quad (1)$$

after the calibration equation of Anand et al. (2003). A detailed explanation of the derivation and error analysis for this new correction can be found in the Data Repository.

Changes in the down-core SST record (ΔT, difference between past and modern SST; Locarnini et al., 2010) and radiative forcing from GHGs (ΔRF, difference between past radiative forcing and preindustrial values) are the foundation of the calculation of past tropical Pacific equilibrium climate sensitivity to radiative forcing. We compare these estimates of past climate sensitivity to model simulations of the LGM to assess the importance of glacial boundary conditions (e.g., ice albedo) in model simulations and discuss the relevance of our results to validating tropical climate sensitivity predicted by climate models.

RESULTS AND DISCUSSION

A number of techniques to calculate the past tropical climate sensitivity parameter (λ) are considered: (1) comparison of the resampled ΔT and ΔRF records at even time steps, (2) comparison of the average glacial and interglacial values for each record, and (3) comparison of the relationship between the amplitude of the coherent bandwidth of each record at 100 k.y. periodicity. Each technique, described in detail below, yields notably similar results [λ = 0.94–1.06 °C (W m^{-2})$^{-1}$].

Although teleconnections with ice-sheet albedo and orbital-scale oscillations in solar radiation play a small role in driving tropical SST at the 100 k.y. periodicity, we first consider radiative forcing by GHGs to be the primary factor for amplifying warm pool SST in the frequency band that dominates the SST record, ~100 k.y. (e.g., Lea, 2004), and later evaluate the role of other glacial boundary conditions for determining tropical climate change. This assumption is the starting point of our analysis for several reasons. First, direct GHG radiative forcing is an order of magnitude greater than that of annual average solar radiation. Using black body calculations, the direct effect of glacial-interglacial GHG changes (combined radiative change of ~2.6 W m^{-2}; IPCC, 2007) on surface temperature is ~0.4 °C while, in comparison, the direct effect of a change in local annual average solar radiation due to changes in eccentricity is ~0.04 °C (or <0.2 W m^{-2}) (Hartmann, 1994). Though insolation changes from an individual season are larger, we consider annual average insolation since our samples record annual average SST. Therefore, though orbital parameters are potential triggers of glacial-interglacial change, they are considered negligible as direct tropical radiation changes at the 100 k.y. periodicity. Further, ice-sheet albedo has a direct radiative effect on surface temperature up to ~2000 km from the southern edge of the ice sheet (Jackson and Broccoli, 2003), still far from the tropics. Ice sheets indirectly influence wind fields, which can impact ocean vertical density structure, mixing, and upwelling (Lee and Poulsen, 2005). However, these effects are minimal for tropical SST at off-equator non-upwelling sites such as ODP Site 871. Finally, frequency analyses of changes in climate parameters suggest that even if orbital variations pace glacial-interglacial cycles, GHG variations are the major forcing of tropical warm pool SST in the late Pleistocene (Lea, 2004). For these reasons, we first assume that GHGs are the primary forcing of past warm pool SST and later consider the role of other changes in glacial boundary conditions when we compare our results to climate simulations of the LGM.

Sea-surface temperature change (ΔT; Fig. 2) was directly related to radiative forcing (ΔRF) using the formula $\Delta T = \lambda \times \Delta R$ (IPCC, 2007; Lea, 2004). The slope of ΔT and ΔRF (method 1) at Site 871 yields a past climate sensitivity parameter (λ_1) of 1.06 ± 0.05 °C (W m^{-2})$^{-1}$ (Fig. 3). The second method for calculating λ uses only the average glacial and interglacial temperatures and radiative forcing as determined from visual inspection of the global benthic oxygen isotope stack (Table DR1 in the Data Repository) and yields a λ_2 of 0.94 ± 0.12 °C (W m^{-2})$^{-1}$. By eliminating transitional periods between glacial and interglacial intervals, this method depends less on the accuracy of the age model and reduces apparent λ by <0.15 °C (W m^{-2})$^{-1}$. The third method compares the relative amplitude in the frequency band most coherent between the temperature and radiative forcing records, the ~100 k.y. band, resulting in a λ_3 of 0.97 °C (W m^{-2})$^{-1}$. Thus, even when other frequency bands are excluded, λ_3 is 92% of λ_1; this result is not surprising given that most of the variance in ΔT and ΔRF is highly coherent and in phase, and occurs in the 100 k.y. frequency band. The

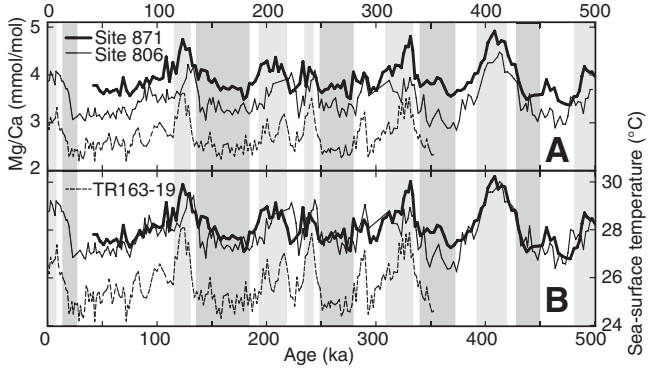

Figure 2. Mg/Ca and sea-surface temperature (SST) records from equatorial Pacific Ocean sites: Ocean Drilling Program (ODP) Site 806 (Medina-Elizalde and Lea, 2005), core TR163-19 (Lea et al., 2000), and ODP Site 871 (this study). A: Measured Mg/Ca records. B: SST calculated with new pre-exponential dissolution correction. Blue and red bars are glacial and interglacial periods, respectively. Sedimentation rate for Site 871 is 1.0 ± 0.1 cm/k.y.

[1]GSA Data Repository item 2013008, sample information and geochemical data from ODP Site 871, with associated ages and sea-surface temperatures, is available online at www.geosociety.org/pubs/ft2013.htm, or on request from editing@geosociety.org or Documents Secretary, GSA, P.O. Box 9140, Boulder, CO 80301, USA.

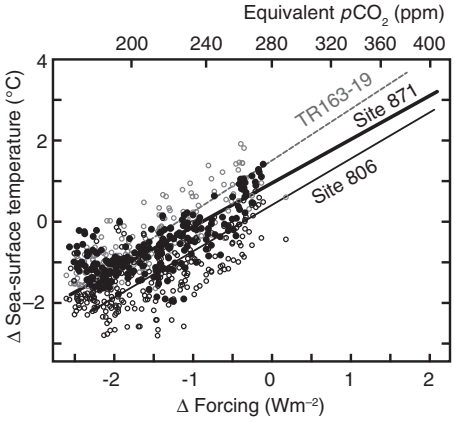

Figure 3. Past climate sensitivity to changes in greenhouse gas (GHG) forcing. The regression (where ΔT is sea-surface temperature change and ΔRF is radiative forcing) for Ocean Drilling Program (ODP) Site 871 is $\Delta T = 1.06\ (\pm 0.05) \times \Delta RF + 0.91\ (\pm 0.08)$, $r^2 = 0.53$; for ODP Site 806 is $\Delta T = 1.12\ (\pm 0.05) \times \Delta RF + 0.38\ (\pm 0.09)$, $r^2 = 0.47$; and for site TR163-19 is $\Delta T = 1.25\ (\pm 0.05) \times \Delta RF + 1.48\ (\pm 0.09)$, $r^2 = 0.70$.

techniques described above give a range of values for λ [0.94–1.06 °C (W m^{-2})$^{-1}$] and, taking into account uncertainties in the climate sensitivity regression and time scale, a total range of 0.82–1.11 °C (W m^{-2})$^{-1}$. This range is equivalent to a temperature change associated with a doubling of GHG concentration of 3.5–3.9 °C (full range, including uncertainty, of 3.03–4.12 °C).

Potential biases in the Site 871 SST record include low sedimentation rate, possible bioturbation, and uncertainties in the dissolution calibration. If a low sedimentation rate or bioturbation reduced the apparent Mg/Ca amplitude at Site 871, the actual climate sensitivity could be greater than we calculate. However, the amplitude similarity between Site 871 benthic $\delta^{18}O$ and the benthic $\delta^{18}O$ stack suggests that bioturbation is not impacting the amplitude of long-time-scale cycles at Site 871 any more severely than at the higher-sedimentation-rate open-ocean sites used in the stack. Our dissolution correction assumed 0.9 mmol/mol (~18%) dissolution at 1255 m water depth. If less dissolution occurred at this depth, or if we had corrected for less dissolution in glacial intervals, the potential past climate sensitivity would be greater [up to 1.29 °C (W m^{-2})$^{-1}$; see the Data Repository]. Each potential bias equates to higher λ and does not resolve the model-data mismatch for past climate sensitivity estimates.

We also calculated past climate sensitivity at other warm-pool tropical Pacific SST records for comparison. As an example, the piecewise technique (method 1) using the new dissolution calibration and the Mg/Ca record from ODP Site 806 (Fig. 1) yields a value for λ_1 of 1.13 ± 0.05 °C (W m^{-2})$^{-1}$. The higher sensitivity at Site 806 than off-equator Site 871 suggests that local ocean dynamics (e.g., equatorial upwelling strength) amplified equatorial SST changes and cooled Site 806 more during glacial intervals. At site TR163-19 in the eastern Pacific (Lea et al., 2000; Fig. 1), SST was even more sensitive [λ_1 = 1.25 ± 0.05 °C (W m^{-2})$^{-1}$] possibly because Site TR163-19 is near an oceanographic front or was influenced by shifts of the Intertropical Convergence Zone (ITCZ) or upwelling changes (Koutavas and Lynch-Stieglitz, 2003).

The climate sensitivity parameter estimated from Site 871 is 0.11–0.39 °C (W m^{-2})$^{-1}$ higher than Paleoclimate Modeling Intercomparison Project Phase II (PMIP2) models suggest for the tropical LGM (Otto-Bliesner et al., 2009; Fig. 4). Comparisons of observation-based estimates of λ to LGM model estimates present an interesting case study because insolation changes and many of the slow feedbacks (e.g., ice sheets) are imposed as model boundary conditions (Otto-Bliesner et al., 2009). The fact that models underestimate the observed tropical cooling when ice sheets and seasonal solar forcing are prescribed implies that the relatively high tropical climate sensitivity we determine is unlikely to be related to neglecting the teleconnections with high-latitude albedo changes due to glaciation or to neglecting the impact of high-latitude insolation changes.

Because LGM model simulations incorporate ice volume, sea level, and GHG concentrations as given fields and make adjustments for deep ocean circulation changes (Otto-Bliesner et al., 2009), the climate sensitivity mismatch between observational and modeled estimates of past sensitivity may be rooted in the way other boundary conditions are treated. In LGM simulations, both vegetation and dust aerosol boundary conditions are prescribed as present-day values. However, cold glacial conditions tend to favor vegetation types with higher albedo and more atmospheric dust (Yue et al., 2011), which cool the climate further during glacial periods. Our results, which reflect the dust forcing feedback, are consistent within error with paleoclimate estimations of the global climate sensitivity parameter when dust is treated as a feedback (Rohling et al., 2012).

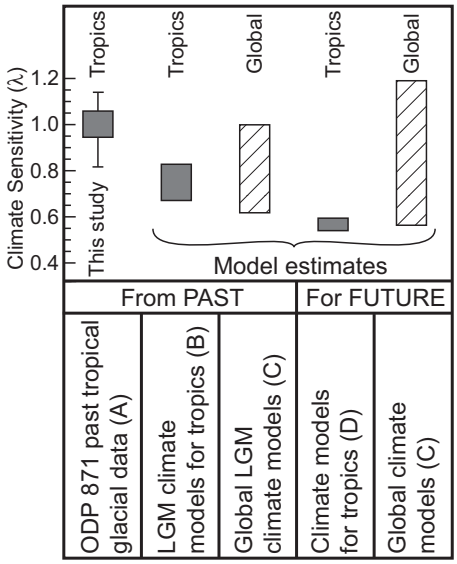

Figure 4. Comparison of climate sensitivity results from this study (paleoclimate data) with tropical and global modeling results for the Last Glacial Maximum (LGM) and future warming. ODP—Ocean Drilling Program; A—this study (with uncertainties); B—Otto-Bliesner et al., 2009; C—IPCC, 2007; D—DiNezio et al., 2009.

Our past tropical climate sensitivity parameter is also 0.37–0.49 °C (W m^{-2})$^{-1}$ higher than predicted by the Coupled Model Intercomparison Project Phase 3 (CMIP3) models of future doubling of CO_2 (DiNezio et al., 2009; Fig. 4). The primary reason for the difference may simply be that our data-based estimates of past climate sensitivity inherently include slow feedbacks related to such components of the Earth system as deep ocean circulation changes or ice-volume changes, which may not be fully realized in climate models. The complexity of simulating the effects of clouds (e.g., Delworth et al., 2006) and other short-term feedback mechanisms may also explain why models of future tropical climate might underestimate climate sensitivity (Knutti and Hegerl, 2008). Such effects are especially important near the equator where cloud-related feedbacks play a large role.

As paleoclimate data directly informs our understanding of the past, it may not be appropriate to scale observational estimates of glacial-interglacial climate sensitivity to future warming scenarios since nonlinear feedbacks add uncertainty to such an extrapolation at low latitudes (Crucifix, 2006). Numerical simulations of climate are needed to accurately estimate future tropical climate sensitivity. Yet, until simulations are able to capture the full range of tropical SST suggested by the paleoclimate data, models may underestimate future climate sensitivity. Resolution of this data-model mismatch in past glacial cycles is required to refine predictions of future climate sensitivity.

SUMMARY

This work shows that past long-term equilibrium climate sensitivity of the tropical Pacific region to forcing by GHG concentration changes is 0.94–1.06 °C (W m^{-2})$^{-1}$, larger than suggested by multi-model projections of either past glacial tropical sensitivity or future tropical sensitivity to doubled CO_2 concentrations. It also shows that a pre-exponential dissolution correction is necessary for accurate reconstructions of past temperature using Mg/Ca ratios from foraminifera. Methodology to construct tropical Pacific temperature records using Mg/Ca in foraminifera will benefit from a more comprehensive core-top calibration from the region, including a greater range of shallow (<1500 m) core-top Mg/Ca data.

Past climate sensitivity calculated in this study focuses on tropical regions and does not represent global equilibrium climate sensitivity. Global and high-latitude climate sensitivities are thought to be larger than that in the tropics (e.g., Holland and Bitz, 2003) due to extreme amplification of climate perturbations where ice-albedo feedbacks operate. Because tropical SSTs are expected to be less responsive to GHG forcing than high-latitude SSTs, our tropical equilibrium sensitivity estimates may be a lower bound for long-term global climate sensitivity.

ACKNOWLEDGMENTS

This research was supported by the Schlanger Fellowship from the Consortium for Ocean Leadership, and by National Science Foundation grant OCE-0902047. We thank the Ocean Drilling Program for providing samples, Jessica Macias and Victor Castro for assistance in sample processing, and anonymous reviewers for constructive comments.

REFERENCES CITED

Anand, P., Elderfield, H., and Conte, M.H., 2003, Calibration of Mg/Ca thermometry in planktonic foraminifera from a sediment trap time series: Paleoceanography, v. 18, doi:10.1029/2002PA000846.

Andreasen, D., and Ravelo, A., 1997, Tropical Pacific Ocean thermocline depth reconstructions for the last glacial maximum: Paleoceanography, v. 12, p. 395–413, doi:10.1029/97PA00822.

Carton, J.A., and Giese, B.S., 2008, A reanalysis of ocean climate using simple ocean data assimilation (SODA): Monthly Weather Review, v. 136, p. 2999–3017, doi:10.1175/2007MWR1978.1.

Crucifix, M., 2006, Does the Last Glacial Maximum constrain climate sensitivity?: Geophysical Research Letters, v. 33, L18701, doi:10.1029/2006GL027137.

Dekens, P., Lea, D., Pak, D., and Spero, H., 2002, Core top calibration of Mg/Ca in tropical foraminifera: Refining paleotemperature estimation: Geochemistry Geophysics Geosystems, v. 3, doi:10.1029/2001GC000200.

Delworth, T., Broccoli, A., Rosati, A., Stouffer, R., Balaji, V., Beesley, J., Cooke, W., Dixon, K., Dunne, J., and Dunne, K., 2006, GFDL's CM2 global coupled climate models. Part I: Formulation and simulation characteristics: Journal of Climate, v. 19, p. 643–674, doi:10.1175/JCLI3629.1.

DiNezio, P.N., Clement, A.C., Vecchi, G.A., Soden, B.J., Kirtman, B.P., and Lee, S.-K., 2009, Climate response of the equatorial Pacific to global warming: Journal of Climate, v. 22, p. 4873–4892, doi:10.1175/2009JCLI2982.1.

Hansen, J., and Sato, M., 2012, Paleoclimate implications for human-made climate change, *in* Berger, A., Mesinger, F., and Šijači, D., eds., Climate Change at the Eve of the Second Decade of the Century: Inferences from Paleoclimate and Regional Aspects: Proceedings of the Milutin Milankovitch 130th Anniversary Symposium: New York, Springer, p. 21–47.

Hartmann, D.L., 1994, Global Physical Climatology: San Diego, California, Academic Press, 411 p.

Holland, M.M., and Bitz, C.M., 2003, Polar amplification of climate change in coupled models: Climate Dynamics, v. 21, p. 221–232, doi:10.1007/s00382-003-0332-6.

IPCC (Intergovernmental Panel on Climate Change; Solomon, S., et al., eds.), 2007, Climate Change 2007: The Physical Science Basis. Contribution of Working Group I to the Fourth Assessment Report of the Intergovernmental Panel on Climate Change, 2007: Cambridge, UK, New York, Cambridge University Press, 996 p.

Jackson, C.S., and Broccoli, A.J., 2003, Orbital forcing of Arctic climate: Mechanisms of climate response and implications for continental glaciation: Climate Dynamics, v. 21, p. 539–557, doi:10.1007/s00382-003-0351-3.

Knutti, R., and Hegerl, G.C., 2008, The equilibrium sensitivity of the Earth's temperature to radiation changes: Nature Geoscience, v. 1, p. 735–743, doi:10.1038/ngeo337.

Koutavas, A., and Lynch-Stieglitz, J., 2003, Glacial-interglacial dynamics of the eastern equatorial Pacific cold tongue-Intertropical Convergence Zone system reconstructed from oxygen isotope records: Paleoceanography, v. 18, doi:10.1029/2003PA000894.

Lea, D., 2004, The 100 000-yr cycle in tropical SST, greenhouse forcing, and climate sensitivity: Journal of Climate, v. 17, p. 2170–2179, doi:10.1175/1520-0442(2004)017<2170:TYCITS>2.0.CO;2.

Lea, D., Pak, D., and Spero, H., 2000, Climate impact of late Quaternary equatorial Pacific sea surface temperature variations: Science, v. 289, p. 1719, doi:10.1126/science.289.5485.1719.

Lee, S.-Y., and Poulsen, C.J., 2005, Tropical Pacific climate response to obliquity forcing in the Pleistocene: Paleoceanography, v. 20, PA4010, doi:10.1029/2005PA001161.

Lisiecki, L.E., and Raymo, M.E., 2005, A Pliocene-Pleistocene stack of 57 globally distributed benthic $\delta^{18}O$ records: Paleoceanography, v. 20, PA1003, doi:10.1029/2004PA001071.

Locarnini, R., Mishonov, A., Antonov, J., Boyer, T., Garcia, H., Baranova, O., Zweng, M., and Johnson, D., 2010, World Ocean Atlas 2009, *in* Levitus, S., ed., National Oceanic and Atmospheric Administration (NOAA) Atlas NESDIS 68: Washington, D.C., U.S. Government Printing Office, 184 p.

Loulergue, L., Schilt, A., Spahni, R., Masson-Delmotte, V., Blunier, T., Lemieux, B., Barnola, J.-M., Raynaud, D., Stocker, T.F., and Chappellaz, J., 2008, Orbital and millennial-scale features of atmospheric CH4 over the past 800,000 years: Nature, v. 453, p. 383–386, doi:10.1038/nature06950.

Medina-Elizalde, M., and Lea, D., 2005, The mid-Pleistocene transition in the Tropical Pacific: Science, v. 310, p. 1009–1012, doi:10.1126/science.1115933.

Mix, A.C., Bard, E., and Schneider, R., 2001, Environmental processes of the ice age: Land, oceans, glaciers (EPILOG): Quaternary Science Reviews, v. 20, p. 627–657, doi:10.1016/S0277-3791(00)00145-1.

Otto-Bliesner, B.L., and 16 others, 2009, A comparison of PMIP2 model simulations and the MARGO proxy reconstruction for tropical sea surface temperatures at last glacial maximum: Climate Dynamics, v. 32, p. 799–815, doi:10.1007/s00382-008-0509-0.

Rohling, E.J., Medina-Elizalde, M., Shepherd, J.G., Siddall, M., and Stanford, J.D., 2012, Sea surface and high-latitude temperature sensitivity to radiative forcing of climate over several glacial cycles: Journal of Climate, v. 25, p. 1635–1656, doi:10.1175/2011JCLI4078.1.

Rosenthal, Y., and Lohmann, G.P., 2002, Accurate estimation of sea surface temperatures using dissolution-corrected calibrations for Mg/Ca paleothermometry: Paleoceanography, v. 17, doi:10.1029/2001PA000749.

Schmittner, A., Urban, N., Shakun, J., and Mahowald, N., 2011, Climate sensitivity estimated from temperature reconstructions of the Last Glacial Maximum: Science, v. 334, p. 1385–1388, doi:10.1126/science.1203513.

Shipboard Scientific Party, 1993, Site 871, *in* Silva, P.I., Haggerty, J., and Rack, R., eds., Proceedings of the Ocean Drilling Program, Initial Reports, vol. 144: College Station, Texas, Ocean Drilling Program, p. 105–144.

Siegenthaler, U., Stocker, T., Monnin, E., Lüthi, D., Schwander, J., Stauffer, B., Raynaud, D., Barnola, J., Fischer, H., and Masson-Delmotte, V., 2005, Stable carbon cycle–climate relationship during the late Pleistocene: Science, v. 310, p. 1313–1317, doi:10.1126/science.1120130.

Waelbroeck, C., Paul, A., Kucera, M., Rosell-Melé, A., Weinelt, M., Schneider, R., Mix, A.C., and 45 others, 2009, Constraints on the magnitude and patterns of ocean cooling at the Last Glacial Maximum: Nature Geoscience, v. 2, p. 127–132, doi:10.1038/ngeo411.

Yue, X., Wang, H., Liao, H., and Jiang, D., 2011, Simulation of the direct radiative effect of mineral dust aerosol on the climate at the Last Glacial Maximum: Journal of Climate, v. 24, p. 843–858, doi:10.1175/2010JCLI3827.1.

Manuscript received 19 March 2012
Revised manuscript received 14 June 2012
Manuscript accepted 18 June 2012

Printed in USA

Late Pleistocene tropical Pacific temperature sensitivity to radiative greenhouse gas forcing

SUPPLEMENTAL MATERIAL

Primary data for this study are from Ocean Drilling Program (ODP) Site 871 at the Limilok Guyot (5º33.13'N, 172º20.66'E, water depth 1255m, (Shipboard Scientific Party, 1993)). The site has a modern annual average SST of 28.8ºC (Locarnini et al., 2010). One sample was taken every 3 cm downcore; ~40-60 *Globigerinoides ruber* (white) tests and 1-5 *Uvigerina spp.* Tests were picked from the 250-355 μm size fraction of each sample.

Samples of the surface mixed-layer foraminifer *G. ruber* were cleaned following established protocols including oxidation and reduction steps (e.g. Boyle and Keigwin 1985/1986; Mashiotta et al., 1999) just as in other studies (Dekens et al, 2002; Lea et al., 2000; Medina-Elizalde and Lea 2005). Mg/Ca ratios were measured using an ICP-OES at the University of California Santa Cruz; 1-σ standard deviation for repeated measurements of an internal foraminifera reference standard is 0.21 mmol/mol, or ~0.5 Cº.

Dissolution Correction

Carbonate shells preferentially lose high-Mg calcite to dissolution with depth; thus a dissolution correction for Mg/Ca must be applied to reconstruct the accurate range of tropical SST (e.g. Brown and Elderfield, 1996; Rosenthal et al., 2000). Since dissolution lowers the Mg/Ca value of the shell and the resulting temperature, one common method to correct for dissolution is to add a specified term to the temperature, depending on the degree of dissolution, commonly associated with the depth of the sediment core (Dekens et al., 2002). For example, applying a correction for dissolution to the published Mg/Ca-based temperature record from ODP Site 806 (Medina-Elizalde and Lea, 2005) using this method (Dekens et al., 2002) produces the range in temperature shown in Fig. DR1-A. Since dissolution affects the Mg/Ca values of the shell, and not the temperature directly, it is more appropriate to correct the Mg/Ca value for dissolution first, before using the exponential relationship (between Mg/Ca and temperature) to estimate temperature, similar in theory to that suggested by Rosenthal et al. (2002).

Our new dissolution correction is applied to measured Mg/Ca values in order to estimate the original surface Mg/Ca value before dissolution occurs at depth. We established a regional depth-based dissolution correction from published modern annual average SST

and core top Mg/Ca data (Broecker and Peng, 1982; Lea et al., 2000; Dekens et al., 2002) from the tropical Pacific warm pool region and create a linear (r^2=0.93) correction for dissolution with depth (Fig. DR1-B) assuming that core-top planktonic foraminifera formed in waters directly over the core location at modern SST. Cold tongue values were excluded since dissolution within the sediments likely increases with large differences in organic matter productivity. While a linear relationship may be an oversimplification, it is a reasonable estimation over the given range of ocean depths and data available. The 'residual' Mg/Ca is calculated from the difference between the calculated and measured Mg/Ca values of *G. ruber* from each core top. For each coretop location, the surface Mg/Ca value was calculated using the modern surface temperature (Locarnini et al., 2010) and the Anand et al. (2003) equation of Mg/Ca = 0.38 e^[0.09*SST]. This equation is indistinguishable from the Dekens et al. (2002) equation at zero water depth. The Mg/Ca (residual) represents the shift in Mg/Ca value that occurs due to dissolution. A simple linear regression against water depth (Fig. DR1B), with errors, yields:

$$Mg/Ca(residual) = 0.26(\pm 0.03) * Depth(km) + 0.54(\pm 0.08).$$

The y-intercept of 0.54 (±0.08) implies that if we extrapolate the regression to the sea surface (zero water depth) there is significant dissolution, which contradicts the idea that dissolution is only a serious problem at depths close to the lysocline and below (Sadekov et al., 2010). However, the shallowest of the sites used in this calibration is 1.6 km; deeper than 1.6 km, the linear regression is constrained by the calibration data, but above 1.6 km, dissolution must actually decrease more quickly, perhaps non-linearly, than the regression fit implies. Thus, the application of this formula to shallow sites must be approached with caution (as explained in more detail below). We use this linear regression formula to develop a complete equation for sea-surface paleotemperature using the depth-based dissolution correction of sediment Mg/Ca to surface Mg/Ca and the exponential Mg/Ca-temperature relationship (Anand et al., 2003). The complete equation for sea-surface paleotemperature, including errors, is:

$$SST = \frac{\ln(\frac{Mg/Ca(surf.)}{0.38(\pm 0.02)})}{0.090(\pm 0.003)},$$

where

$$Mg/Ca(surf.) = Mg/Ca(measured) + 0.26(\pm 0.03) * Depth(km) + 0.54(\pm 0.08),$$

or, for an overall equation for Mg/Ca:

$$Mg/Ca_{ruber}(mmol/mol) = -0.26(\pm 0.03) * Depth(km) - 0.54(\pm 0.08) + 0.38(\pm 0.02) * e^{0.09(\pm 0.003)*T}.$$

Conceptually, this dissolution correction shifts the exponential Mg/Ca-temperature calibration curve vertically (lower) through Mg/Ca-SST-space rather than adding a (horizontal) constant temperature correction as in previous work (Fig. DR1-D). When uncertainties in the depth-dissolution regression are propagated in the temperature calibration, the dissolution correction could add up to 1.3 Cº of uncertainty to the SST calculation. In this study the dissolution correction is assumed to be unchanging through time and shifts all temperature estimates by approximately the same amount. Further work is warranted to minimize this uncertainty at shallow water depths.

Since the calibration equation derived above is based on coretop data from sites that are deeper than 1.6 km, the question is: How should we then apply this calibration to data from ODP Site 871, which has a shallower water depth of 1.3 km? Our preferred method is conservative, and simply uses the original linear regression and extrapolates the core-top calibration from 1.6 km to 1.3 km water depth (Fig. DR1B). This method results in smaller amplitudes of SST (Fig. DR1-C) compared to the traditional method where an offset correction is applied to the SST values (e.g., Dekens et al., 2007, Fig. DR1-A). Furthermore, compared to other methods explained below to extrapolate the calibration to 1.3 km, this conservative method using our new calibration yields the lowest climate sensitivity values (open square in Fig. DR1-B).

Another approach to extrapolating the calibration to the depth of our core site (1.3 km) assumes that the Mg/Ca offset at zero water depth is zero (Fig. DR1B). At one extreme, this is represented by a second regression from the shallowest depth at which there is calibration data (1.6 km) and through the origin (though the artificial sudden change in slope at 1.6 km water depth seems unlikely). This yields corrected Mg/Ca values that are 0.14 mmol/mol higher than the first approach. This small difference is within the measured Mg/Ca error, suggesting that the original calibration is sufficient for this depth.

At the opposite extreme, we can assume that there was no dissolution shallower than 1.6 km (Fig. DR1B). In this case there would be no dissolution correction at ODP site 871. The resulting climate sensitivity estimates would then be higher than any formulation that attempts to correct for dissolution (λ = 1.29 ºC $(W\,m^{-2})^{-1}$), and the estimates of previous interglacial temperatures in the western Pacific would be consistently ~2 Cº cooler than modern, rendering this scenario unlikely.

The dissolution calibration also depends on the paleotemperature equation used to calculate surface Mg/Ca (from which the residual is calculated, Fig. DR1B). We tried 7 different equations (Anand et al., 2003; Elderfield and Ganssen, 2000; Hastings et al., 2001; Hendry et al., 2009; McConnell and Thunell, 2005; Pak et al., 2004; Regenberg et

al., 2009), though most cluster around the original Anand equation. Equations that do not correct for dissolution result in cooler absolute temperatures, higher glacial-interglacial amplitude of change, and higher climate sensitivity, compared to our new calibration that corrects for significant dissolution.

Overall, directly applying our new calibration equation, which assumes that the Mg/Ca-residual due to dissolution changes linearly with depth (Fig. DR1B) and extrapolates that linear relationship to 1.2 km (the depth of ODP Site 871), produces the lowest climate sensitivity values compared to other methods that either ignore dissolution or correct for dissolution using a different approach. Even these lowest estimates of climate sensitivity are higher than those predicted by models; this main point is a robust result that is not undermined by uncertainties in the dissolution correction.

In general, our new calibration has the overall effect of, given a change in measured Mg/Ca values, reducing the calculated amplitude of SST compared to the commonly used correction (Dekens et al., 2002). This difference between the dissolution corrections becomes greater at deeper water depths (Fig. DR2). Overall, our new Mg-based dissolution-corrected temperature record demonstrates the smaller amplitude of glacial-interglacial temperature change compared to other calibrations when applied to Mg/Ca records in the tropics.

When our new Mg-based dissolution correction is applied to existing long Mg/Ca records from the tropical Pacific (Site 806B and TR163-19) the resulting cold glacial temperatures are warmer than previous studies suggested while the interglacial temperatures are relatively unchanged (Fig. DR3) from published temperature estimates (Lea, 2004; Medina-Elizalde and Lea, 2005).

For this study we use the foraminifera species *Globigerinoides ruber* (white). No differentiation was made among morphotypes of *G. ruber*, though small differences have been shown to exist in Mg/Ca-SST calibrations (Steinke et al., 2005). This choice is reasonable given the morphotypes of *G. ruber* are gradational (Sadekov et al., 2008) and temperature differences among morphotypes are likely to be small (Bolton et al., 2011) in areas with a deep thermocline and minimal upwelling.

Tropical Climate Sensitivity Error Calculations

Tropical climate sensitivity is determined by comparing the forcing associated with greenhouse gas concentrations (CO_2 and CH_4) and the change in temperature at tropical ODP Site 871 (Fig. DR4). The correlation coefficient (Pearson's r) for the Site 871 temperature record and the atmospheric CO_2 record is 0.74 while the correlation for the Site 871 temperature record and the atmospheric CH_4 record is 0.67. Comparison of this

climate sensitivity parameter with models is made in the text under the Results and Discussion section. Error in the climate sensitivity parameter incorporates 95% confidence intervals in the dissolution correction and the RMA regressions of ΔSST and ΔRF. The 95% confidence interval for the resulting climate sensitivity parameter is 0.82 – 1.11 ºC $(W\,m^{-2})^{-1}$) and for the climate sensitivity (Fig. 4) is 3.03 - 4.12 Cº. The non-zero intercept in each regression (Fig. 3) is due to past interglacial timeperiods that were slightly warmer than pre-industrial temperatures (Lea, 2004; Hansen and Sato, 2011).

The Role of Dynamics

While some small amount of surface temperature change at Site 871 may be due to shifts in the local temperature gradients, it is unlikely that local dynamics could have much of an impact on SST since the gradients in the western Pacific warm pool are weak, less than 1ºC change over 6º of latitude (670 km). Furthermore, during the glacial periods, SST at Site 871 was warmer than at Site 806; a reversal in the direction of the gradient between the two sites cannot be explained by expansion or contraction of modern gradients. Rather it implies that dynamics, such as upwelling, may have cooled temperatures at equatorial Site 806 slightly during glacial periods. Cooler temperatures at Site 806 on the equator may support the notion that Site 871 is a more ideal location for examining western Pacific warm pool heat flux adjustments to radiative forcing.

Radiative Forcing Calculations

For carbon dioxide, we use (Ramaswamy et al., 2001):

$$\Delta F_{CO2} = 4.841 \ln([CO_2]/[CO_2]_0) + 0.0906 (\sqrt{[CO_2]} - \sqrt{[CO_2]_0}).$$

For methane, we use (Ramaswamy et al., 2001):

$$\Delta F_{CH4} = 0.036 (\sqrt{[CH_4]} - \sqrt{[CH4]_0}) - [0.47 \ln\{1 + 2.01\times10^{-5} ([CH_4] [N_2O]_0)^{0.75} + 5.31\times10^{-15} [CH_4] ([CH_4] [N_2O]_0)^{1.52}\}] - [0.47 \ln\{1 + 2.01\times10^{-5} ([CH_4]_0 [N_2O]_0)^{0.75} + 5.31\times10^{-15} [CH_4]_0 ([CH4]_0 [N_2O]_0)^{1.52}\}]$$

where $[CO_2]_0$ = 280 ppmv, $[CH_4]_0$ = 700 ppb, and $[N_2O]_0$ = 280 ppb.

The total radiative forcing is $\Delta F_{TOT} = \Delta F_{CO2} + \Delta F_{CH4}$. As in other studies (Lea, 2004), past changes in N_2O are ignored since N_2O has a relatively small radiative influence and lacks a continuous record.

Time Scale

Each Mg/Ca record treated in this study is associated with a benthic $\delta^{18}O$ record at a similar resolution from the same core. Modern bottom-water temperature at Site 871 is 3.5ºC, salinity 34.5 (Locarnini et al., 2010). These $\delta^{18}O$ records covary in time and space and are aligned with a global 'stack' of benthic $\delta^{18}O$ data. For this study, we generated the benthic $\delta^{18}O$ record for Site 871 using *Uvigerina spp*. from the same samples and size fraction as the Site 871 temperature record. From the 250-355 μm size fraction, 1-3 individual shells were analyzed, at a resolution of one sample every 3 cm. Samples were analyzed at the University of California Stable Isotope Laboratory using a Fisons PRISM mass spectrometer with a common acid bath carbonate preparation system. Standard error for 46 measurements of an internal CM05 $\delta^{18}O$ standard was ±0.05‰. The benthic $\delta^{18}O$ data from Site 806 and TR163-19 is from *Uvigerina spp.* and *C. wuellerstorfi* from previous studies (Bickert et al., 1993; Lea et al., 2002) at a similar temporal resolution. Site-specific benthic $\delta^{18}O$ records were visually aligned (Fig. DR5) with a common timescale using glacial and interglacial maxima (Lisiecki and Raymo, 2005) with only small corrections in alignment with Analyseries software (Palliard et al., 1996).

On average the Site 871 temperature record seems to lead global benthic $\delta^{18}O$ (LR04 stack) by about 9(± 2) kyr at the 100-kyr frequency. At other frequencies there does not appear to be any lead between the signals. The temperature lead varies among terminations: at T-II (~130 kya) SST leads, though at other terminations SST and the benthic $\delta^{18}O$ stack covary. The early temperature increase in MIS 6 is also seen at other west Pacific sites (e.g. de Villiers, 2003). The out-of-phase behavior between SST and benthic $\delta^{18}O$ record is inconsequential to our calculation of climate sensitivity since we are comparing SST and CO_2 records which are in-phase within error at orbital frequencies. The fact that all three approaches for calculating climate sensitivity provide the same result within error further suggests that the correlation with CO_2 is good. To check this observation, we also removed the data prior to 150 ka, retaining the parts of the Site 871 SST record that look similar to more common tropical sites, and re-calculated the sensitivity. The result is $\lambda = 1.08$ ºC $(W\,m^{-2})^{-1}$, the same result as when data from Termination II is included, within error.

Regression

The relationships for regression through temperature and radiative forcing data are developed using the Reduced Major Axis (RMA) approach (1000 iterations; Sokal and Rohlf, 2011) which is reasonable when the independent variable x is measured with error (Fig. DR6).

SUPPLEMENTARY MATERIAL REFERENCES

Anand, P., Elderfield, H., and Conte, M.H., 2003, Calibration of Mg/Ca thermometry in planktonic foraminifera from a sediment trap time series: Paleoceanography, v. 18, no. 2, doi: 10.1029/2002PA000846.

Bickert, T., Berger, W., Burke, S., and Schmidt, H., 1993, Late Quaternary stable isotope record of Cibicidoides wuellerstorfi from the Ontong Java Plateau: en.scientificcommons.org.

Bolton, A., Baker, J.A., Dunbar, G.B., Carter, L., Smith, E.G.C., and Neil, H.L., 2011, Environmental versus biological controls on Mg/Ca variability in Globigerinoides ruber(white) from core top and plankton tow samples in the southwest Pacific Ocean: Paleoceanography, v. 26, no. 2, p. PA2219, doi: 10.1029/2010PA001924.

Boyle, E., and Keigwin, L., 1985, Comparison of Atlantic and Pacific paleochemical records for the last 215,000 years: Changes in deep ocean circulation and chemical inventories: Earth and Planetary Science Letters, v. 76, no. 1-2, p. 135–150.

Broecker, W.S., and Peng, T.H., 1982, Tracers in the Sea: Lamont-Doherty Geological Observatory, Palisades, NY.

Brown, S., and Elderfield, H., 1996, Variations in Mg/Ca and Sr/Ca ratios of planktonic foraminifera caused by postdepositional dissolution: Evidence of shallow Mg-dependent dissolution: Paleoceanography, v. 11, no. 5, p. 543–551.

Dekens, P., Lea, D., Pak, D., and Spero, H., 2002, Core top calibration of Mg/Ca in tropical foraminifera: Refining paleotemperature estimation: Geochemistry Geophysics Geosystems, v. 3, p. 1022, doi: 10.1029/2001GC000200.

Elderfield, H., and Ganssen, G., 2000, Past temperature and δ18O of surface ocean waters inferred from foraminiferal Mg/Ca ratios: Nature, v. 405, no. 6785, p. 442–445.

Hastings, D.W., Kienast, M., Steinke, S., and Whitko, A., 2001), A comparison of three independent paleotemperature estimates from a high resolution record of deglacial SST records in the tropical South China Sea, Eos Trans. AGU, 82(47), Fall Meet. Suppl., Abstract PP12B-10.

Hendry, K.R., Rickaby, R.E.M., Meredith, M.P., and Elderfield, H., 2009, Controls on stable isotope and trace metal uptake in Neogloboquadrina pachyderma (sinistral) from an Antarctic sea-ice environment: Earth and Planetary Science Letters, v. 278, no. 1-2, p. 67–77, doi: 10.1016/j.epsl.2008.11.026.

Lea, D., 2004, The 100 000-yr cycle in tropical SST, greenhouse forcing, and climate sensitivity: Journal of Climate, v. 17, no. 11, p. 2170–2179.

Lea, D., Martin, P., Pak, D., and Spero, H., 2002, Reconstructing a 350 ky history of sea level using planktonic Mg/Ca and oxygen isotope records from a Cocos Ridge core: Quaternary Science Reviews, v. 21, no. 1-3, p. 283–293.

Lea, D., Pak, D., and Spero, H., 2000, Climate impact of late Quaternary equatorial Pacific sea surface temperature variations: Science, v. 289, no. 5485, p. 1719.

Lisiecki, L.E., and Raymo, M.E., 2005, A Pliocene-Pleistocene stack of 57 globally distributed benthic $\delta^{18}O$ records: Paleoceanography, v. 20, no. 1, p. PA1003, doi: 10.1029/2004PA001071.

Locarnini, R., Mishonov, A., Antonov, J., Boyer, T., Garcia, H., Baranova, O., Zweng, M., and Johnson, D., 2010, World Ocean Atlas 2009, *in* Levitus, S. ed. NOAA Atlas NESDIS 68, U.S. Government Printing Office, Washington, D.C.

Mashiotta, T., Lea, D., and Spero, H., 1999, Glacial-interglacial changes in Subantarctic sea surface temperature and [delta] 18O-water using foraminiferal Mg: Earth and Planetary Science Letters, v. 170, no. 4, p. 417–432.

McConnell, M.C., and Thunell, R.C., 2005, Calibration of the planktonic foraminiferal Mg/Ca paleothermometer: Sediment trap results from the Guaymas Basin, Gulf of California: Paleoceanography, v. 20, no. 2, doi: 10.1029/2004PA001077.

Medina-Elizalde, M., and Lea, D., 2005, The mid-Pleistocene transition in the Tropical Pacific: Science, v. 310, no. 5750, p. 1009.

Pak, D.K., Lea, D.W., and Kennett, J.P., 2004, Seasonal and interannual variation in Santa Barbara Basin water temperatures observed in sediment trap foraminiferal Mg/Ca: Geochemistry Geophysics Geosystems, v. 5, p. Q12008.

Palliard, D., Labeyrie, L., and Yiou, P., 1996, Macintosh program performs time-series analysis: Eos Trans. AGU 77, 379 p.

Ramaswamy, V., Boucher, O., Haigh, J., Hauglustaine, D., Haywood, J., Myhre, G., Nakajima, T., Shi, G., Solomon, S., and Betts, R., 2001, Radiative forcing of climate change:.

Regenberg, M., Steph, S., Nürnberg, D., Tiedemann, R., and Garbe-Schönberg, D., 2009, Calibrating Mg/Ca ratios of multiple planktonic foraminiferal species with δ18O-calcification temperatures: Paleothermometry for the upper water column: Earth and

Planetary Science Letters, v. 278, no. 3-4, p. 324–336, doi: 10.1016/j.epsl.2008.12.019.

Rosenthal, Y., and Lohmann, G.P., 2002, Accurate estimation of sea surface temperatures using dissolution-corrected calibrations for Mg/Ca paleothermometry: Paleoceanography, v. 17, no. 3, p. 1044.

Rosenthal, Y., Lohmann, G., Lohmann, K., and Sherrell, R., 2000, Incorporation and preservation of Mg in Globigerinoides sacculifer: Implications for reconstructing the temperature and 18O/16O of seawater: Paleoceanography, v. 15, no. 1, p. 135–145.

Sadekov, A., Eggins, S.M., De Deckker, P., and Kroon, D., 2008, Uncertainties in seawater thermometry deriving from intratest and intertest Mg/Ca variability in Globigerinoides ruber: Paleoceanography, v. 23, no. 1, doi: 10.1029/2007PA001452.

Sadekov, A.Y., Eggins, S.M., Klinkhammer, G.P., and Rosenthal, Y., 2010, Effects of seafloor and laboratory dissolution on the Mg/Ca composition of Globigerinoides sacculifer and Orbulina universa tests — A laser ablation ICPMS microanalysis perspective: Earth and Planetary Science Letters, v. 292, no. 3-4, p. 312–324, doi: 10.1016/j.epsl.2010.01.039.

Shipboard Scientific Party, 1993, Site 871, *in* Silva, P.I., Haggerty, J., and Rack, R. eds. Proceedings of the Ocean Drilling Program, Initial Reports, Vol. 144, Ocean Drilling Program, p. 105–144.

Sokal, R.R., and Rohlf, F.J., 2011, Biometry: The Principles and Practices of Statistics in Biological Research: W. H. Freeman, New York, NY.

Steinke, S., Chiu, H.-Y., Yu, P.-S., Shen, C.-C., Löwemark, L., Mii, H.-S., and Chen, M.-T., 2005, Mg/Ca ratios of two Globigerinoides ruber(white) morphotypes: Implications for reconstructing past tropical/subtropical surface water conditions: Geochemistry Geophysics Geosystems, v. 6, no. 11, p. Q11005, doi: 10.1029/2005GC000926.

de Villiers, S. (2003) Dissolution effects on foraminiferal Mg/Ca records of sea surface temperature in the western equatorial Pacific. *Paleoceanography*, **18**:3.

SUPPLEMENTARY FIGURE CAPTIONS

Figure DR1: Comparison of calibration techniques using Site 806B *G. ruber* Mg/Ca record (Medina-Elizalde and Lea, 2005), which has a glacial-interglacial (G-IG) amplitude of 1.06 mmol/mol as an example. (A) Previous calibration technique correcting temperatures for dissolution by adding an offset to the derived temperature (Dekens et al., 2002) results in a G-IG amplitude of 3.2 Cº. (B) The relationship between water depth and Mg/Ca residual, from core top data (filled circles) outside the Cold Tongue where dissolution may be greater. The relationship is $Mg/Ca_{residual} = 0.26$ (±0.03)*Depth(km) + 0.54 (±0.08). $R^2 = 0.93$. Core top data and locations are presented in Dekens et al. (2002), Tables 1 and 4. The equation is extrapolated 12% beyond the shallowest core to the depth of Site 871 (open square). Open circles are possibilities that cannot be eliminated, though each produces even higher climate sensitivity and greater data-model mismatch. (C). The new calibration, derived in this study, to correct Mg/Ca for dissolution first before calculating paleotemperature, results in a G-IG amplitude of 2.5 Cº. (D) The calibration for this study shifts the surface Mg/Ca-temperature curve vertically while other calibrations appear to shift the curve horizontally.

Figure DR2: Comparison of Mg/Ca-corrected calibration (this study, solid lines) and previous calibration (Dekens et al., 2002). Using the new Mg-based dissolution correction results in a smaller range of tropical Pacific glacial-interglacial temperatures for cores at any depth.

Figure DR3: Existing Mg/Ca records (Medina-Elizalde and Lea, 2005; Lea et al., 2000; black lines) corrected using the Mg-based dissolution correction as described (solid lines). In general, our new calibration shifts glacial temperatures toward warmer values, while interglacials remain unchanged.

Figure S4: Site 871 SST compared through time with atmospheric greenhouse gas concentrations. Blue and red vertical bars are glacial and interglacial times, respectively.

Figure DR5: Benthic $\delta^{18}O$ records measured from Site 871, Site 806, and TR163-19 mentioned in the text compared to a global stack (Lisiecki and Raymo, 2005) for temporal alignment and age determination. Blue and red vertical bars are glacial and interglacial times, respectively. The correlation coefficient (Pearson's r) for the Site 871 benthic $\delta^{18}O$ record and the benthic LR04 stack is 0.79. Tie points are indicated by black diamonds.

Figure DR6: Regressions through data from TR163-19, Site 871, and Site 806 with regression errors plotted.

Table DR1: Glacial and Interglacial periods visually identified from global benthic oxygen-isotope stack (Lisiecki and Raymo, 2005).

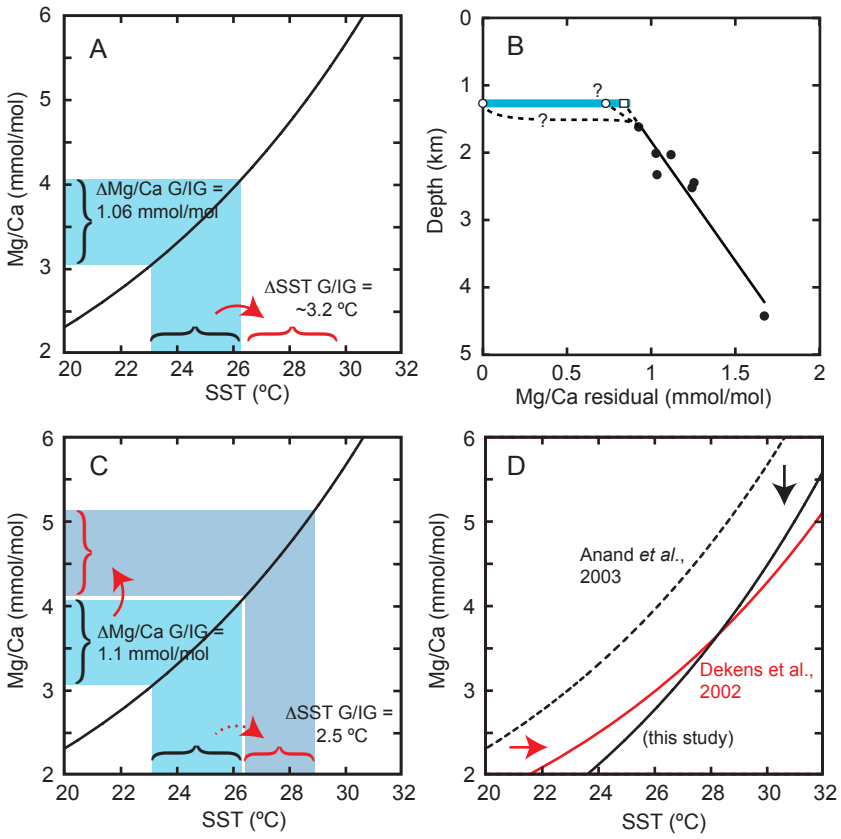
A
Mg/Ca (mmol/mol)
SST (ºC)
ΔMg/Ca G/IG =
1.06 mmol/mol
ΔSST G/IG =
~3.2 ºC
B
Depth (km)
Mg/Ca residual (mmol/mol)
?
?
C
Mg/Ca (mmol/mol)
SST (ºC)
ΔMg/Ca G/IG =
1.1 mmol/mol
ΔSST G/IG =
2.5 ºC
D
Mg/Ca (mmol/mol)
SST (ºC)
Anand et al.,
2003
Dekens et al.,
2002
(this study)

Figure DR1

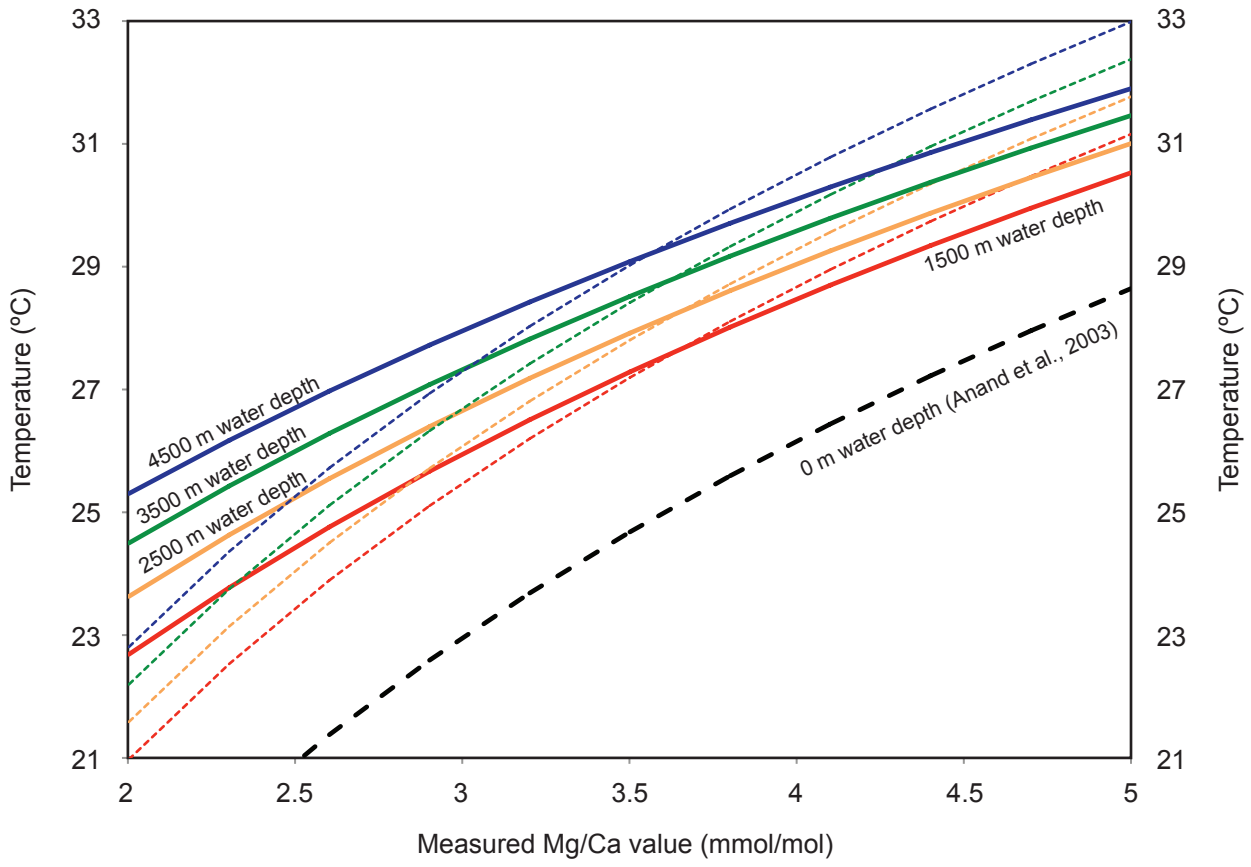
33
31
29
27
25
23
21
Temperature (°C)
2
2.5
3
3.5
4
4.5
5
Measured Mg/Ca value (mmol/mol)
4500 m water depth
3500 m water depth
2500 m water depth
1500 m water depth
0 m water depth (Anand et al., 2003)

Figure DR2

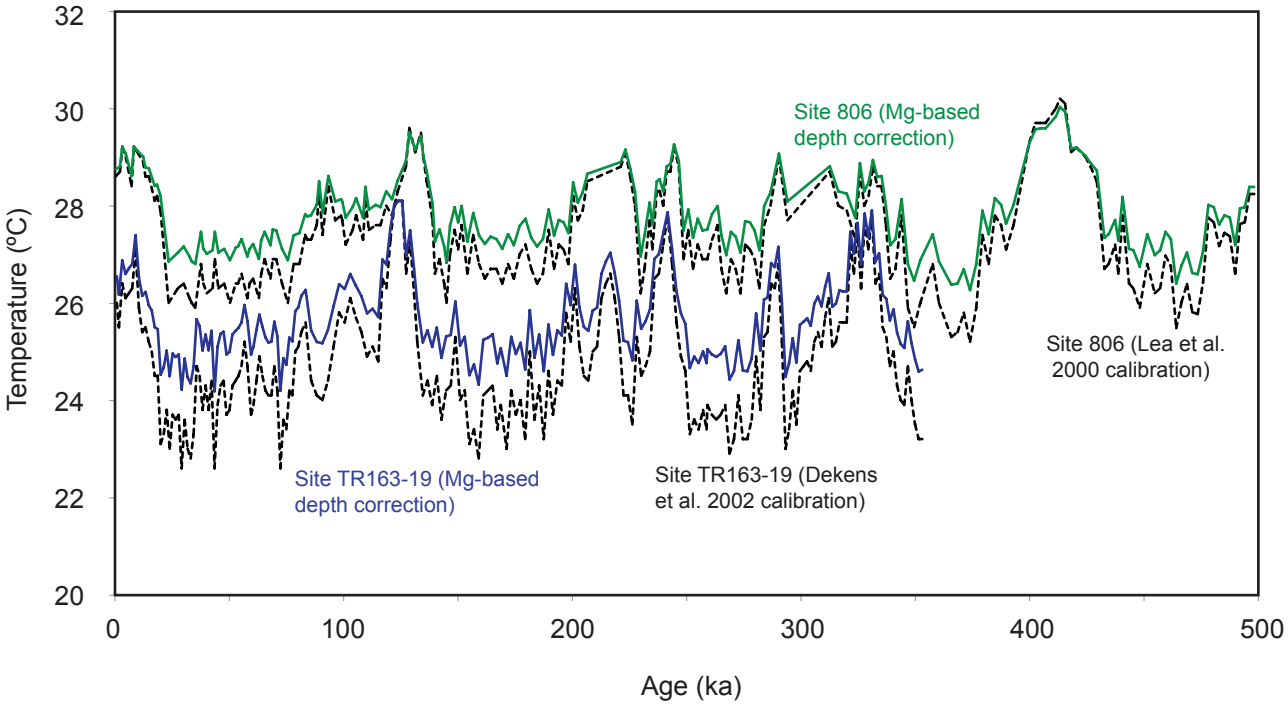
32
30
28
26
24
22
20
Temperature (ºC)
0
100
200
300
400
500
Age (ka)
Site 806 (Mg-based depth correction)
Site 806 (Lea et al. 2000 calibration)
Site TR163-19 (Mg-based depth correction)
Site TR163-19 (Dekens et al. 2002 calibration)

Figure DR3

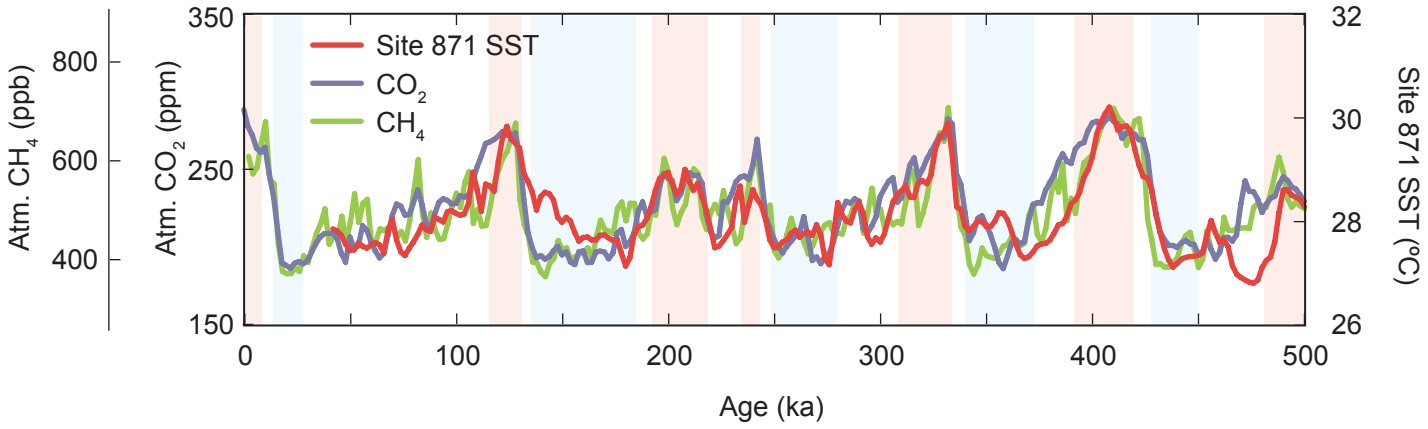
Site 871 SST
CO2
CH4
Atm. CH4 (ppb)
Atm. CO2 (ppm)
Site 871 SST (°C)
Age (ka)
800
600
400
350
250
150
32
30
28
26
0
100
200
300
400
500

Figure DR4

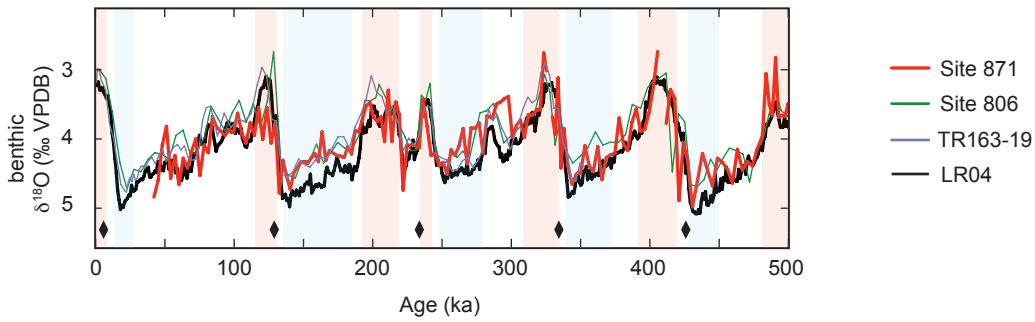
benthic
δ18O (‰ VPDB)
3
4
5
0
100
200
300
400
500
Age (ka)
Site 871
Site 806
TR163-19
LR04

Figure DR5

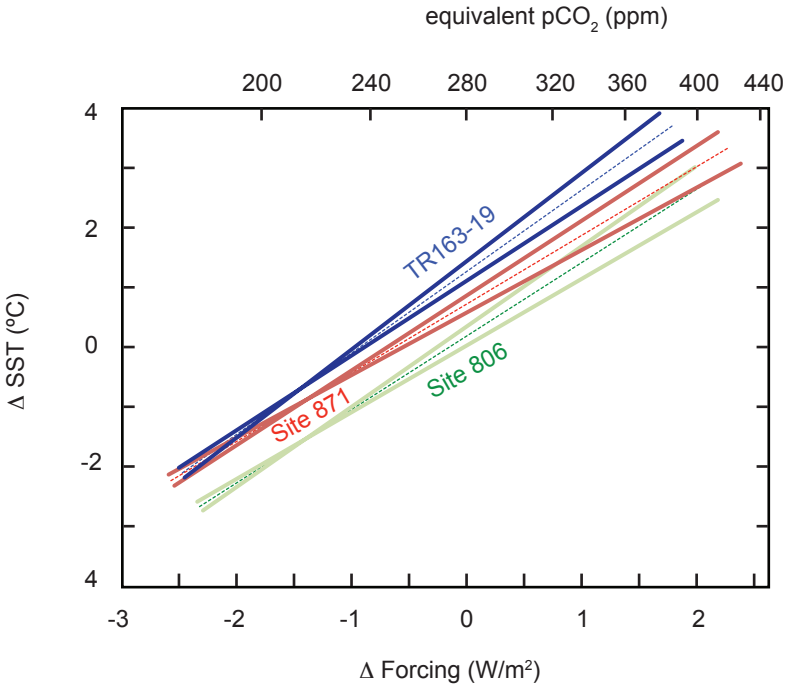
equivalent pCO2 (ppm)
200
240
280
320
360
400
440
4
2
0
-2
4
Δ SST (°C)
TR163-19
Site 871
Site 806
-3
-2
-1
0
1
2
Δ Forcing (W/m2)

Figure DR6

Table DR1.

Glacial or Interglacial period	Termination (kya)	Inception (kya)
Stage 1	0	11
Stage 2	17	28
Stage 5e	114	130
Stage 6	135	185
Stage 7(a)	192	220
Stage 7(b)	234	243
Stage 8	248	280
Stage 9	308	334
Stage 10	340	373
Stage 11	391	421
Stage 12	428	472
Stage 13	482	498

Data Repository, ODP Site 871

Units and Abbreviations:
mbsf (meters below sea floor)
Sample listed as: ODP Site, Hole, Core, Type, Section, Interval (cm)
d18O (Uvigerina spp. d18O (o/oo))
Age (kya)
Mg/Ca (G. ruber, white, mmol/mol)
SST (sea-surface temperature)
Blank values (N/A)

mbsf	Site	Hole	Core	Type	Section	Interval		d18O	Age(kya)	Mg/Ca	SST
0.01	871	B	1	H	1	1	3	4.18	0.00	3.858	28.0
0.04	871	B	1	H	1	4	6	4.35	2.87	4.072	28.5
0.07	871	B	1	H	1	7	9	4.00	5.89	3.839	27.9
0.1	871	B	1	H	1	10	12	4.08	8.91	3.962	28.2
0.13	871	B	1	H	1	13	15	3.96	11.93	4.073	28.5
0.16	871	B	1	H	1	16	18	4.43	14.95	3.669	27.5
0.19	871	B	1	H	1	19	21	3.56	17.97	3.942	28.2
0.22	871	B	1	H	1	22	24	4.18	20.99	4.109	28.6
0.25	871	B	1	H	1	25	27	4.05	24.01	3.952	28.2
0.28	871	B	1	H	1	28	30	4.41	27.03	3.621	27.4
0.31	871	B	1	H	1	31	33	4.44	30.05	3.897	28.1
0.34	871	B	1	H	1	34	36	3.29	33.07	3.867	28.0
0.37	871	B	1	H	1	37	39	4.20	36.09	4.119	28.6
0.4	871	B	1	H	1	40	42	3.61	39.11	3.944	28.2
0.43	871	B	1	H	1	43	45	4.84	42.13	3.786	27.8
0.46	871	B	1	H	1	46	48	4.60	45.15	3.784	27.8
0.49	871	B	1	H	1	49	51	4.09	48.16	3.669	27.5
0.52	871	B	1	H	1	52	54	3.82	51.18	3.610	27.4
0.55	871	B	1	H	1	55	57	4.57	54.20	3.702	27.6
0.58	871	B	1	H	1	58	60	4.24	57.22	3.639	27.5
0.61	871	B	1	H	1	61	63	4.66	60.24	3.675	27.6
0.64	871	B	1	H	1	64	66	4.28	63.26	3.705	27.6
0.67	871	B	1	H	1	67	69	4.42	66.28	3.582	27.3
0.7	871	B	1	H	1	70	72	4.18	69.30	3.948	28.2
0.73	871	B	1	H	1	73	75	4.00	72.32	3.682	27.6
0.76	871	B	1	H	1	76	78	4.53	75.34	3.570	27.3
0.79	871	B	1	H	1	79	81	4.09	78.36	3.661	27.5
0.82	871	B	1	H	1	82	84	4.20	81.38	3.730	27.7
0.85	871	B	1	H	1	85	87	3.68	84.40	3.857	28.0
0.88	871	B	1	H	1	88	90	3.84	87.42	3.741	27.7
0.91	871	B	1	H	1	91	93	3.89	90.44	3.933	28.2
0.94	871	B	1	H	1	94	96	3.95	93.46	3.829	27.9
0.97	871	B	1	H	1	97	99	3.87	96.48	3.969	28.3
1	871	B	1	H	1	100	102	3.91	99.50	3.933	28.2
1.03	871	B	1	H	1	103	105	3.63	102.52	3.907	28.1
1.06	871	B	1	H	1	106	108	3.92	105.53	3.941	28.2
1.09	871	B	1	H	1	109	111	4.06	108.55	4.380	29.2

mbsf	Site	Hole	Core	Type	Section	Interval		d18O	Age(kya)	Mg/Ca	SST
1.12	871	B	1	H	1	112	114	3.77	111.57	3.868	28.0
1.15	871	B	1	H	1	115	117	3.95	114.59	4.266	28.9
1.18	871	B	1	H	1	118	120	3.55	117.61	4.040	28.4
1.21	871	B	1	H	1	121	123	4.01	120.63	4.473	29.4
1.24	871	B	1	H	1	124	126	3.55	123.65	4.746	29.9
1.27	871	B	1	H	1	127	129	4.06	126.67	4.533	29.5
1.3	871	B	1	H	1	130	132	3.77	129.69	4.558	29.5
1.33	871	B	1	H	1	133	135	4.78	132.54	4.198	28.8
1.36	871	B	1	H	1	136	138	4.31	135.19	4.196	28.8
1.39	871	B	1	H	1	139	141	4.54	137.84	3.912	28.1
1.42	871	B	1	H	1	142	144	4.73	140.49	4.113	28.6
1.45	871	B	1	H	1	145	147	4.48	143.14	4.100	28.5
1.48	871	B	1	H	1	148	150	4.41	145.79	4.077	28.5
1.5	871	B	1	H	2	0	1	4.35	147.56	3.898	28.1
1.53	871	B	1	H	2	3	4	4.33	150.21	3.843	28.0
1.56	871	B	1	H	2	6	7	4.36	152.86	3.922	28.1
1.59	871	B	1	H	2	9	10	4.28	155.51	3.791	27.8
1.62	871	B	1	H	2	12	13	4.21	158.16	3.685	27.6
1.65	871	B	1	H	2	15	16	4.33	160.81	3.754	27.7
1.68	871	B	1	H	2	18	19	3.90	163.46	3.714	27.6
1.71	871	B	1	H	2	21	22	4.31	166.11	3.708	27.6
1.74	871	B	1	H	2	24	25	4.17	168.76	3.768	27.8
1.77	871	B	1	H	2	27	28	3.86	171.41	(N/A)	(N/A)
1.8	871	B	1	H	2	30	31	4.24	174.06	3.704	27.6
1.83	871	B	1	H	2	33	34	4.25	176.71	3.725	27.7
1.86	871	B	1	H	2	36	37	4.27	179.36	3.494	27.1
1.89	871	B	1	H	2	39	40	4.11	182.00	3.555	27.3
1.92	871	B	1	H	2	42	43	4.22	184.65	3.829	27.9
1.95	871	B	1	H	2	45	46	3.88	187.30	3.813	27.9
1.98	871	B	1	H	2	48	49	3.90	189.95	3.878	28.0
2.01	871	B	1	H	2	51	52	3.71	192.60	4.010	28.3
2.04	871	B	1	H	2	54	55	3.52	195.25	4.220	28.8
2.07	871	B	1	H	2	57	58	3.48	197.90	4.247	28.9
2.1	871	B	1	H	2	60	61	3.69	200.55	4.295	29.0
2.13	871	B	1	H	2	63	64	3.75	203.20	4.082	28.5
2.16	871	B	1	H	2	66	67	3.68	205.85	4.099	28.5
2.19	871	B	1	H	2	69	70	4.04	208.50	4.371	29.1
2.22	871	B	1	H	2	72	73	3.30	211.15	4.075	28.5
2.25	871	B	1	H	2	75	76	4.04	213.80	4.218	28.8
2.28	871	B	1	H	2	78	79	3.47	216.45	4.035	28.4
2.31	871	B	1	H	2	81	82	3.65	219.10	3.897	28.1
2.34	871	B	1	H	2	84	85	4.74	221.90	3.628	27.4
2.37	871	B	1	H	2	87	88	4.09	224.78	3.677	27.6
2.4	871	B	1	H	2	90	93	(N/A)	227.66	(N/A)	(N/A)
2.43	871	B	1	H	2	93	94	4.10	230.55	3.821	27.9
2.46	871	B	1	H	2	96	97	4.13	233.43	4.281	28.9

mbsf	Site	Hole	Core	Type	Section	Interval		d18O	Age(kya)	Mg/Ca	SST
2.49	871	B	1	H	2	99	100	3.43	236.31	3.765	27.8
2.52	871	B	1	H	2	102	103	3.82	239.19	4.164	28.7
2.55	871	B	1	H	2	105	106	4.24	242.08	4.040	28.4
2.58	871	B	1	H	2	108	109	4.21	244.96	3.972	28.3
2.61	871	B	1	H	2	111	112	4.39	247.84	3.706	27.6
2.64	871	B	1	H	2	114	115	4.34	250.73	3.632	27.4
2.67	871	B	1	H	2	117	118	4.51	253.61	3.697	27.6
2.7	871	B	1	H	2	120	121	4.16	256.49	3.713	27.6
2.73	871	B	1	H	2	123	124	4.24	259.37	3.815	27.9
2.76	871	B	1	H	2	126	127	4.10	262.26	3.718	27.7
2.79	871	B	1	H	2	129	130	3.85	265.14	3.795	27.8
2.82	871	B	1	H	2	132	133	4.36	268.02	3.732	27.7
2.85	871	B	1	H	2	135	136	3.84	270.91	3.882	28.0
2.88	871	B	1	H	2	138	139	3.85	273.79	3.552	27.2
2.91	871	B	1	H	2	141	142	3.77	276.67	3.506	27.1
2.94	871	B	1	H	2	144	145	4.21	279.55	4.067	28.5
2.97	871	B	1	H	2	147	148	3.67	282.44	3.884	28.1
3.01	871	B	1	H	3	1	3	3.70	286.28	3.835	27.9
3.04	871	B	1	H	3	4	6	3.50	289.16	4.044	28.4
3.07	871	B	1	H	3	7	9	3.47	292.05	3.947	28.2
3.1	871	B	1	H	3	10	12	3.42	294.93	3.642	27.5
3.13	871	B	1	H	3	13	15	3.39	297.81	3.744	27.7
3.16	871	B	1	H	3	16	18	3.98	300.69	3.679	27.6
3.19	871	B	1	H	3	19	21	3.81	303.58	3.865	28.0
3.22	871	B	1	H	3	22	24	3.73	306.46	4.058	28.5
3.25	871	B	1	H	3	25	27	3.98	309.34	4.098	28.5
3.28	871	B	1	H	3	28	30	3.65	312.23	4.180	28.7
3.31	871	B	1	H	3	31	33	3.66	315.11	3.995	28.3
3.34	871	B	1	H	3	34	36	3.59	317.99	4.209	28.8
3.37	871	B	1	H	3	37	39	3.58	320.87	4.203	28.8
3.4	871	B	1	H	3	40	42	2.76	323.29	4.154	28.7
3.43	871	B	1	H	3	43	45	3.02	325.38	4.448	29.3
3.46	871	B	1	H	3	46	48	(N/A)	327.46	4.605	29.6
3.49	871	B	1	H	3	49	51	3.68	329.54	4.590	29.6
3.52	871	B	1	H	3	52	54	3.93	331.62	4.809	30.0
3.55	871	B	1	H	3	55	57	3.12	333.71	4.534	29.5
3.58	871	B	1	H	3	58	60	4.42	335.79	3.928	28.2
3.61	871	B	1	H	3	61	63	3.85	337.87	3.996	28.3
3.64	871	B	1	H	3	64	66	4.38	340.67	3.764	27.8
3.67	871	B	1	H	3	67	69	4.65	343.75	3.816	27.9
3.7	871	B	1	H	3	70	72	4.51	346.84	3.885	28.1
3.73	871	B	1	H	3	73	75	4.49	349.93	3.816	27.9
3.76	871	B	1	H	3	76	78	4.10	353.01	3.821	27.9
3.79	871	B	1	H	3	79	81	4.39	356.10	3.950	28.2
3.82	871	B	1	H	3	82	84	4.47	359.19	3.915	28.1
3.85	871	B	1	H	3	85	87	4.11	362.27	3.765	27.8

mbsf	Site	Hole	Core	Type	Section	Interval		d18O	Age(kya)	Mg/Ca	SST
3.88	871	B	1	H	3	88	90	4.59	365.36	3.608	27.4
3.91	871	B	1	H	3	91	93	4.27	368.45	3.559	27.3
3.94	871	B	1	H	3	94	96	4.23	371.53	3.606	27.4
3.97	871	B	1	H	3	97	99	4.21	374.62	3.683	27.6
4	871	B	1	H	3	100	102	3.70	377.71	3.680	27.6
4.03	871	B	1	H	3	103	105	4.07	380.79	3.722	27.7
4.06	871	B	1	H	3	106	108	4.17	383.88	3.841	28.0
4.09	871	B	1	H	3	109	111	3.76	386.97	3.846	28.0
4.12	871	B	1	H	3	112	114	3.57	390.05	4.023	28.4
4.15	871	B	1	H	3	115	117	3.89	393.14	4.047	28.4
4.18	871	B	1	H	3	118	120	3.86	396.23	4.255	28.9
4.21	871	B	1	H	3	121	123	3.62	399.31	4.342	29.1
4.24	871	B	1	H	3	124	126	3.25	402.40	4.678	29.8
4.27	871	B	1	H	3	127	129	2.74	405.49	4.807	30.0
4.3	871	B	1	H	3	130	132	(N/A)	408.57	4.918	30.2
4.33	871	B	1	H	3	133	135	3.78	411.66	4.649	29.7
4.36	871	B	1	H	3	136	138	3.29	414.75	4.720	29.9
4.39	871	B	1	H	3	139	141	3.42	417.83	4.692	29.8
4.42	871	B	1	H	3	142	144	4.89	420.92	4.406	29.2
4.45	871	B	1	H	3	145	147	4.05	424.01	4.228	28.8
4.48	871	B	1	H	3	148	150	4.32	427.09	4.227	28.8
4.51	871	B	1	H	4	1	3	4.98	430.64	3.864	28.0
4.54	871	B	1	H	4	4	6	4.60	434.24	3.623	27.4
4.57	871	B	1	H	4	7	9	4.21	437.84	3.490	27.1
4.6	871	B	1	H	4	10	12	4.45	441.44	3.561	27.3
4.63	871	B	1	H	4	13	15	4.68	445.04	3.584	27.3
4.66	871	B	1	H	4	16	18	4.28	448.64	3.586	27.3
4.69	871	B	1	H	4	19	21	4.34	452.24	3.603	27.4
4.72	871	B	1	H	4	22	24	4.44	455.84	3.906	28.1
4.75	871	B	1	H	4	25	27	4.64	459.44	3.684	27.6
4.78	871	B	1	H	4	28	30	4.15	463.04	3.731	27.7
4.81	871	B	1	H	4	31	33	4.45	466.64	3.469	27.0
4.84	871	B	1	H	4	34	36	4.33	470.24	3.423	26.9
4.87	871	B	1	H	4	37	39	4.39	473.85	3.391	26.8
4.9	871	B	1	H	4	40	42	4.14	477.45	3.379	26.8
4.93	871	B	1	H	4	43	45	3.96	481.05	3.549	27.2
4.96	871	B	1	H	4	46	48	3.06	483.70	3.560	27.3
4.99	871	B	1	H	4	49	51	3.50	485.98	3.676	27.6
5.02	871	B	1	H	4	52	54	3.66	488.26	3.978	28.3
5.05	871	B	1	H	4	55	57	2.83	490.54	4.179	28.7
5.08	871	B	1	H	4	58	60	3.69	492.82	4.100	28.5
5.11	871	B	1	H	4	61	63	3.66	495.10	4.061	28.5
5.14	871	B	1	H	4	64	66	3.67	497.38	4.066	28.5
5.17	871	B	1	H	4	67	69	3.49	499.66	3.992	28.3
5.2	871	B	1	H	4	70	72	3.88	501.95	3.929	28.2
5.23	871	B	1	H	4	73	75	3.83	504.23	3.912	28.1

mbsf	Site	Hole	Core	Type	Section	Interval		d18O	Age(kya)	Mg/Ca	SST
5.26	871	B	1	H	4	76	78	3.76	506.51	3.821	27.9
5.29	871	B	1	H	4	79	81	4.17	508.79	3.752	27.7
5.32	871	B	1	H	4	82	84	4.14	511.07	3.940	28.2
5.35	871	B	1	H	4	85	87	3.85	513.35	4.101	28.5
5.38	871	B	1	H	4	88	90	4.08	515.63	3.981	28.3
5.41	871	B	1	H	4	91	93	4.05	517.91	3.972	28.3
5.44	871	B	1	H	4	94	96	4.15	520.19	3.994	28.3
5.47	871	B	1	H	4	97	99	3.38	522.61	3.768	27.8
5.5	871	B	1	H	4	100	102	4.07	526.25	3.881	28.0
5.53	871	B	1	H	4	103	105	3.78	529.88	3.486	27.1
5.56	871	B	1	H	4	106	108	4.29	533.51	3.593	27.3
5.59	871	B	1	H	4	109	111	4.23	537.15	3.528	27.2